2018 IEEE-RAS 18th International Conference on Humanoid Robots (Humanoids)
Beijing, China, November 6-9, 2018

Reliably Segmenting Motion Reversals of a Rigid-IMU Cluster using Screw-based Invariants *

Rakesh Krishnan[1,2], Silvia Cruciani[1], Elena Gutierrez-Farewik[3], Niclas Björsell[2] and Christian Smith[1]

***Abstract*—Human-robot interaction (HRI) is moving towards the human-robot synchronization challenge. In robots like exoskeletons, this challenge translates to the reliable motion segmentation problem using wearable devices. Therefore, our paper explores the possibility of segmenting the motion reversals of a rigid-IMU cluster using screw-based invariants. Moreover, we evaluate the reliability of this framework with regard to the sensor placement, speed and type of motion. Overall, our results show that the screw-based invariants can reliably segment the motion reversals of a rigid-IMU cluster.**

I. Introduction

For successful intervention in rehabilitation robotics, the algorithms that drive the HRI are required to detect, react and adapt quickly to changes in user intention [1]. Despite this need, current practices in HRI seldom incorporates the knowledge of human posture into the decision process [2]. Consequently, reliable motion tracking and segmentation based on wearable devices is a fundamental problem in robot-assisted rehabilitation [3]. Therefore, this work focusses on the problem of segmenting the motion reversals of a rigid-IMU cluster using screw-based invariants (see Fig 1). Here, by motion reversals we mean that both forward and reverse motions are exact geometric reversals as shown in Fig 4-A and 4-B.

Reliability is the measure of consistency or repeatability in the data analysis. Moreover, high computational reliability is a pre-requisite for robot-assisted rehabilitation to yield consistent results [4]. Furthermore, in robot-assisted rehabilitation, it is desired that the computational framework is generalizable and platform-invariant [1], [4]. However, such a framework is still a work in progress, as it presents a formidable challenge to extract and interpret the parameters in a meaningful manner [4].

Solutions in the state-of-the-art rehabilitation technology use motion capture or video analysis; however, such solutions cannot be generalized to a real-time and real-world setting [5]. Alternatively, there are inertial measurement units (IMUs) which can measure its own movement by the inertial principle [6]. In comparison to standard motion analysis systems, IMUs are advantageous as they are: affordable, occlusion-free and have increased capture volume [4], [7]. Although IMUs are a viable alternative, their use remains largely unexplored as a biofeedback modality in rehabilitation robotics [1], [6]. Therefore, in the context of HRI, there is a need for an IMU-based computational framework [6].

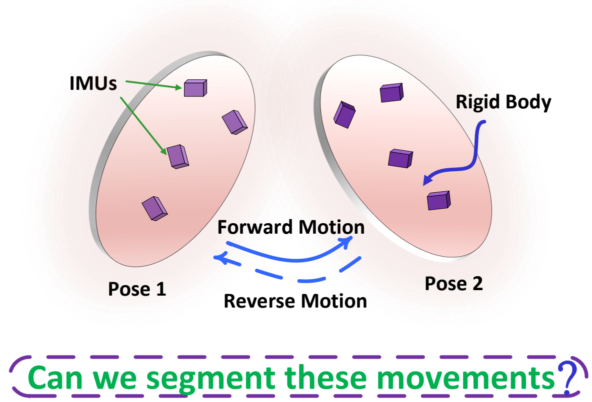

Figure 1: The figure illustrates the main research question which is to segment motion reversals of a rigid body with a cluster of inertial measurement units (IMUs) attached to it. This segmentation is demonstrated by the results in Section VI-A.

Importantly, recent studies have shown that there are several confounding factors that affect the reliability of the IMU processing [8]. These factors are namely: type of motion, speed of execution, magnetic environment, hardware errors, motion protocols and post-processing [5], [8]. Additionally in IMUs, the choice of the underlying kinematic model for information processing will in turn affect the reliability of the extracted parameters [8]. Many of the existing studies have been extensively carried out using human motion. It is well known that human motion has high inter-trial variability. Unlike human motions, robot motions are highly repeatable, their speeds can be carefully controlled and a variety of motions can be tested in a carefully controlled setting. Therefore, to establish a reliable ground-truth, our work explores the reliability of segmenting the motion reversals of a rigid IMU cluster which is guided by a humanoid robot.

*This work was supported by the (AAL Call 6) AXO-SUIT project
[1] Robotics, Perception & Learning (RPL), KTH (Royal Institute of Technology), Stockholm, Sweden rkth@kth.se
[2] Department of Electronics, Mathematics and Natural Sciences, University of Gävle, Gävle, Sweden
[3] KTH Engineering Sciences, Mechanics, Royal Institute of Technology (KTH), Stockholm, Sweden

Our present work addresses several of the above factors in detail. Mainly, the effect of sensor placement, speed and type of motion on segmentation reliability are explored in detail. In our paper, we extend the rigid-body invariants proposed by De Schutter in [9] to IMUs. Importantly, as this framework is coordinate-free, the effect of sensor placement or the choice of kinematic model on reliability can be ruled out. In fact, our earlier work demonstrates that this invariant framework can reliably extract and segment movement features from motion capture data [10].

We open our paper with a brief literature review in Section II. Then, we introduce the screw-based invariants in Section III. Later on, we present the experimental section of our study in Section IV. The results of our experiments are in Section V and Section VI. Furthermore, the main result of our study which is motion segmentation is detailed in Section VI-A, which is accompanied by reliability evaluation of the screw-based invariants in Section VI-B and Section VI-C. We present the conclusions of our study in Section VII.

II. Brief Literature Survey

Motion segmentation algorithms aim to precisely locate the start and end-points of a movement series, which is important for both rehabilitation technology and practice [11]. However, doing so from physical sensors is very challenging [12]. Moreover, there is limited work on motion segmentation using IMUs. To situate our contribution, we present here a brief summary of the relevant literature.

For gesture recognition, Fod et al. [12] present a movement classification framework using perceptuo-motor primitives. Similarly, Lin et al. in [11] present a two-stage online segmentation protocol based on the velocity features and stochastic modeling [11]. The study by Aoki et al. [13], reformulates the motion segmentation as a classification problem. This study uses the absolute value of angular velocities to train a k-NN classifier. Another related work presents SoSaLe-invariants which aims to recover the invariants from a Cartesian trajectory extracted from a video-feed [14]. However, in the context of IMUs, due to poor recovery of Cartesian trajectory, this framework is unsuitable [7]. Therefore, our current work explores the possibility of reliably extracting these motion segments from the IMU data using the screw-based invariants [9], [10].

In motion analysis, many recent surveys summarise the use of IMUs in walking, upper-body and full-body motions [5]–[7]. During a squat task in human subjects, the lower limb kinematics was derived by a single IMU [15]. However, such a framework is limiting for segmentation of three-dimensional movements spanning several IMUs [15]. In gait analysis, uni-axial gyroscopes have been used to detect various gait events [6], [16]. However, the data from tri-axial gyroscopes are complex and need different computational analysis [16]. In our previous work [10], we explored the previously less studied problem of motion segmentation using the kinematic invariants based on motion capture data [12]. However, this framework has never been explored using IMU sensors which we present below.

III. Screw-based Invariants: Theory and Information Processing

The building block of our kinematic information processing is the body-fixed twist representation, which is a 6D vector,

$$\boldsymbol{\eta} = \begin{bmatrix} \boldsymbol{\omega} \\ \mathbf{v} \end{bmatrix}. \tag{1}$$

Here, $\boldsymbol{\omega}$ and $\mathbf{v}$ are the angular and the linear velocities of the body-fixed frame with respect to the global-fixed frame which is expressed in the body-fixed frame. This choice of the reference frame is motivated by two practical reasons. First, the global-fixed frame for IMU processing is the gravity-frame. Extracting the gravity-frame solely by the IMU information is challenging as it leads to multiple solutions [6]. Second, IMUs are internally-referenced sensors [6], which means that by choosing a mathematical framework close to the natural coordinates of the sensors, we can possibly enhance the reliability of the motion segmentation.

From the time history of $\boldsymbol{\eta}$ in (1), the two geometric invariants ω_1 and v_1 can be extracted [9]. These variables describe the motions of the twist-axis, and they are defined as

$$\omega_1 = \boldsymbol{\omega} \cdot \mathbf{e_x}, \quad \text{and} \quad v_1 = \mathbf{v} \cdot \mathbf{e_x}. \tag{2}$$

Here, $\mathbf{e_x}$ is the unit vector representing the twist-axis. The signs of ω_1, v_1 and $\mathbf{e_x}$ in turn depend on the nature of motion [9]. Unlike $\boldsymbol{\omega}$, $\mathbf{v}$ does depend on the choice of the body-fixed coordinate system; therefore, v_1 needs to be compensated accordingly [9].

Mainly, the invariants in (2) can be used to compare movements of different amplitudes and speed [9]. The following time and amplitude normalizations make this possible,

$$\bar{\omega}_1(\bar{t}) = \frac{\omega_1(t)t_f}{\Theta}, \quad \text{and} \quad \bar{v}_1(\bar{t}) = \frac{v_1(t)t_f}{L}. \tag{3}$$

Here, $\bar{t} = \frac{t}{t_f}$ represents dimensionless time, where t_f being the final time. Additionally, $\Theta = \int_0^{t_f} |\omega_1| dt$ and $L = \int_0^{t_f} |v_1| dt$ are the angular and linear scale magnitudes. Note that the higher-order invariants in [9] are currently excluded from analysis as they are sensitive to noise [10].

Note that it is only the tri-axial gyroscopes of the IMU that directly gives information regarding $\boldsymbol{\omega}$ in (1). However, the information about $\mathbf{v}$ in (1) needs to be estimated from the tri-axial accelerometers using a two-step process. First, as the accelerometers simultaneously sense both acceleration due to motion and gravity, the acceleration due to gravity must be compensated. Hence, the second sub-problem is to estimate the velocity from this gravity-compensated acceleration. This presents a non-trivial research question–as a naive integration of acceleration leads to velocity-drift [6]. The next two subsections explore these two sub-problems in detail.

A. Gravity Compensation

To compensate for the gravity component, it is necessary to estimate the orientation of the IMU body-fixed frame $\{\mathbf{X_B}, \mathbf{Y_B}, \mathbf{Z_B}\}$ with respect to the earth-fixed gravity frame $\{\mathbf{X_A}, \mathbf{Y_A}, \mathbf{Z_A}\}$. Let $\hat{q} \in \mathbb{R}^4$ be the generalized unit quaternion. Consider a Eucledian vector $\mathbf{r_A} \in \mathbb{R}^4$ in frame A which is transformed to frame B by,

$$\mathbf{r_B} = \hat{q} \circ \mathbf{r_A} \circ \hat{q}^*, \tag{4}$$

here, the operator $(\circ)$ represents quaternion multiplication and $\hat{q}^*$ is the quaternion conjugate. This quaternion can be estimated by solving the following equation [3],

$$\hat{\omega} = 2\hat{q}^* \circ \dot{\hat{q}}. \tag{5}$$

Here, $\hat{\omega}$ is the quaternion representing the angular velocity vector $\boldsymbol{\omega}$. To estimate the acceleration due to motion $\mathbf{a}$, the component due to the gravity is compensated by,

$$\mathbf{a} = \mathbf{a_B} - \mathbf{R_A^B} \mathbf{a_g}. \tag{6}$$

Here, $\mathbf{a_B}$ is the raw accelerometer data and $\mathbf{a_g}$ is the acceleration due to gravity. The orientation matrix $\mathbf{R_A^B}$ is computed from the estimated quaternion $\hat{q}$ in (5). In the section below we present the integration of the gravity compensated acceleration $\mathbf{a}$.

B. Drift-free Integrator

Recall that simple integration of the acceleration leads to the accumulation of the integration error which results in drift [7]. Few studies have used Fourier-based methods for drift-free integration [15], [17]. These methods are unsuitable for our study as our motions are far more complex and are three-dimensional, thus violating preconditions for the Fourier-based integration. Therefore, we present a leaky integrator to address this sub-problem. Unlike the Euler integrator, its leaky counterpart purposefully forgets a part of the previous output of the integrator; thereby, avoiding drift. This integrator at time instant k is expressed as,

$$y(k) = \alpha y(k-1) + (1-\alpha)x(k), \tag{7}$$

here, $\alpha \in [0, 1]$ is the forgetting factor and $x(k)$ is the instantaneous input to the integrator. The choice of α is further detailed in Section V.

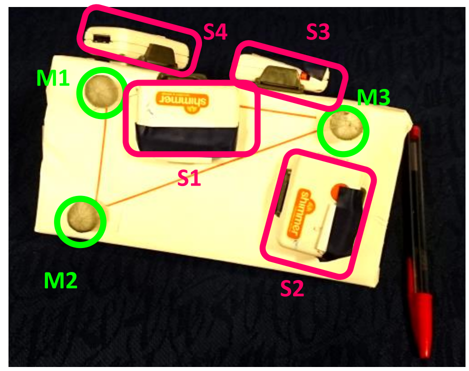

Figure 2: The figure shows the optical markers (M1-M3) placed on a wooden object together with the IMU sensors (S1-S4).

IV. Experiments and Data Processing

The experiments for our study are divided into two parts. First, we aim to arrive at the best choice of the leaky integrator coefficient α in (7). Second, we aim to extract the screw-based invariants of a rigid-IMU cluster, which is guided by a humanoid robot. The motion capture and robot kinematic data respectively act as a ground-truth for our first and second set of experiments. In the robot experiments, we aim to evaluate the effect of the type and the speed of motion on the reliability of the extracted screw-based invariants.

Four Shimmer3 IMU units were used for the data collection during both of the experiments. Each Shimmer3 IMU unit has a tri-axial gyroscope ($\pm$ 500 dps), a tri-axial low-noise accelerometer ($\pm$ 2 g) and a tri-axial magnetometer ($\pm$ 1.9 Ga). The data was streamed via bluetooth and collected on a Dell Latitude Laptop with the ConsensysPRO software at a rate of 120 Hz. Each IMU was individually calibrated using the Shimmer 9-DOF calibration interface. After the experiments, the data from the cluster of IMU sensors were synchronised offline using the ConsensysPRO software. Note that the quaternion estimation in (5) is already custom implemented in the ConsensysPRO interface using the MARG (magnetic, angular-rate, gravity) algorithm [3]. Later on, all the collected data was processed offline. During the offline processing all kinematic data was filtered using a zero-phase Butterworth low-pass filter with cut-off frequency of 6 Hz.

A. Experiment I: IMU with Motion Capture

As illustrated in Fig 2, a wooden object was chosen for motion tacking. On this object, three passive markers (M1-M3) were attached forming a right-angled triad. Four Shimmer3 IMUs were attached in a random fashion. This was to rule out the effect of sensor placement on the data analysis. The motion capture was performed at a rate of 120 frames per second (fps), using an OptiTrack Motive system with 17 camera units.

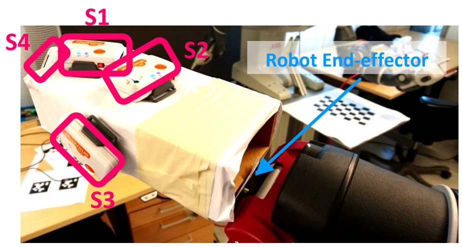

Figure 3: Illustrates the placement of the IMU sensor cluster (S1-S4) rigidly attached to the wooden object placed on the Baxter's end-effector.

Four different movements were performed using a hand-held wooden object as shown in Fig 2. The movements are 1) Vertical Abduction-Adduction, 2) Horizontal Abduction-Adduction, 3) Flexion-Extension, and 4) Random movements. Except for the random set of movements, all other movements were repeated 10 times. For a brief description of these movement definitions please refer to [10].

Mainly, through Experiment I, we aim to motivate the choice of the leaky integrator coefficient α in (7). Therefore, with reference to Fig 2, from the passive markers (M1-M3), the centroid triad velocity $\mathbf{C_v}$ was computed using the forward difference approximation. Later on, the velocity of each IMU $\mathbf{v}$ was computed from the accelerometer data, using the leaky integrator in (7). From these computed velocities, the mean velocity of the IMU cluster $\mathbf{v_m}$ was computed. The results of Experiment I is presented in Section V.

B. Experiment II: IMU with Baxter Robot

For our second set of experiments the same wooden object in Experiment I was mounted with IMU sensors (S1-S4) using double-sided tape. This rigid-IMU cluster was fastened on the Baxter robot's gripper with paper-tape (see Fig 3). The Baxter is a dual-arm humanoid robot with 7-DOF in each arm. Only the right-arm of the Baxter was used in the experiments. The body-fixed twist of the end-effector frame was recorded at a rate of 120 Hz.

Recall that the main aim of the Experiment II is to segment the motion reversals of a rigid-IMU cluster using the screw-based invariants. To evaluate this possibility, we choose two basic motions, namely: vertical abduction-adduction and horizontal abduction-adduction. The joint-S1 of the Baxter drives the vertical abduction-adduction which leads to the forward and reverse motions in the Y-Z plane of the Baxter workspace (see Fig 4). Similarly, the joint-S0 of the Baxter drives the motion in the X-Y plane of the Baxter workspace resulting in the horizontal abduction-adduction (see Fig 4). Note that the maximum available joint speed of these motors are 2.0 rad/sec, however, for safety reasons the movements were always kept at a lower speed. Additionally, to evaluate the effect of the speed on

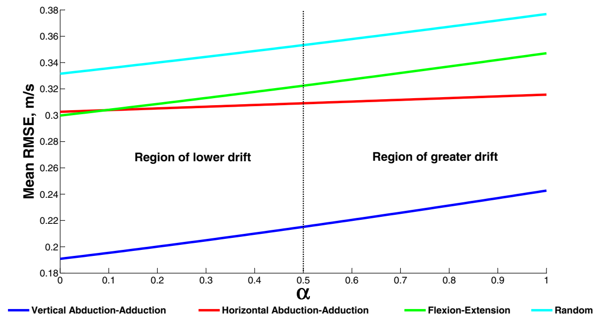

Figure 5: The figure plots the RMSE values in (8). Various activities verified include: 1) Vertical Abduction-Adduction (0.2087 m/s), 2) Horizontal Abduction-Adduction (0.2819 m/s), 3) Flexion-Extension (0.2988 m/s), 4) Random (0.3129 m/s). The velocities mentioned in the brackets include mean of $\|\mathbf{C_v}\|$ for each task.

the reliability of the invariants the basic motions were performed with three different speed ratios, namely: slow (0.1), medium (0.25) and fast (0.4). Each of the basic motion types at a specific speed were repeated ten times in a loop.

To evaluate the effect of motion-type on the reliability of extracted screw-based invariants, we have chosen two advanced motions (see Fig 4). Mainly, a helical-type and lemniscate trajectories were chosen. Note that as these motions are fairly complex; therefore, motion segmentation is not a priority. Due to the complexity of these motions, they were recorded by manually guiding the robot's end-effector through the desired path. Later on, these trajectories were played back ten times each. The results of Experiment II are in Section VI.

V. Results and Discussion: Experiment I

In this section, we present the results of Experiment I in which we compare the IMU with motion capture data. To investigate the best choice of α, we vary α in its range $[0, 1]$. For this purpose, we compute the root mean square error (RMSE) between $\|\mathbf{C_v}\|$ and $\|\mathbf{v_m}\|$,

$$RMSE = \sqrt{\frac{\sum_{n=1}^{N} (\|\mathbf{C_v}\| - \|\mathbf{v_m}\|)^2}{N}}. \tag{8}$$

Fig 5 illustrates the computed RMSE values for the four different motion types. Interestingly, we can see a uniform trend in the mean RMSE values from Fig 5. This is not surprising, as the value of α increases, the integrator forgets less leading to increased drift. However, the intercept of the line is correlated with the mean velocity of the trial. This is why the overall mean RMSE plot for vertical abduction-adduction starts much lower than other trials. Therefore, by choosing $\alpha = 0$ we would get the lowest possible RMSE; however, at the price of zero integration-effect. By selecting $\alpha = 0.5$, a balance between integration-effect and error can be obtained. Note that due to the forgetting factor, the

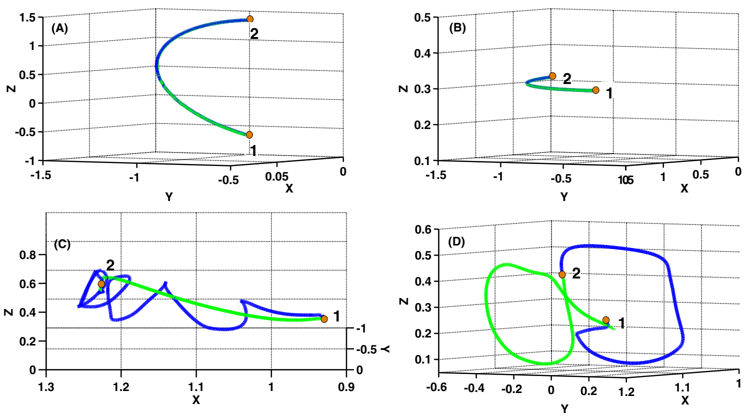

Figure 4: The figure shows the end-effector trajectories for the four robot motions (A) Vertical Abduction-Adduction, (B) Horizontal Abduction-Adduction, (C) Helical trajectory and (D) Lemniscate trajectory. The respective forward motions start from the point 1 and end in 2 (blue). Similarly, the reverse motions start at 2 and end in 1 (green).

leaky integrator is poor at integrating high acceleration data. In the next section, we present the results from Experiment II.

VI. Results and Discussion: Experiment II

This section opens by presenting the main results of our study which is motion segmentation (see Section VI-A). Furthermore, we analyse the reliability of these screw-based invariants in Section VI-B and Section VI-C. Note that during data analysis, it was found that the data from sensor-S2 is faulty. Hence, we skip the analysis of sensor-S2.

A. Motion Segmentation

The main aim of our paper is to reliably segment the motion reversals of the rigid-IMU cluster in Fig 3. This is achieved by using the screw-based geometric invariants presented in (3). During the vertical abduction-adduction task (see Fig 6), the waveforms of $\bar{\omega}_1$ for all the IMU sensors and the robot kinematics clearly superimpose. Irrespective of the speed of motion, the transition from vertical abduction to adduction is clearly marked by reversals of $\bar{\omega}_1$. This is a fundamental property of the screw-based invariants [9].

However, the waveforms of $\bar{v}_1$ in Fig 6 show only a moderate agreement. Mainly, the invariant $\bar{v}_1$ undergoes multiple stages of information processing. Therefore, the error due to estimation and numerical processing adds up leading to large variation. Additionally, the electromagnetic fluctuation due to the robot hardware might affect the accuracy of the orientation estimation. Currently, due to the non-linear and time-varying nature of the numerical processing; this error cannot be exactly quantified [8]. Contrastingly, $\bar{\omega}_1$ undergoes minimal processing, which might explain its excellent agreement. Results are similar for the horizontal abduction-adduction trials (see Fig 7).

For complex motions, the extracted invariants are presented in Fig 8. However, segmenting them is very challenging as the constituent parts of these movements are not exact geometric reversals. In the next two subsections, we present the reliability analysis of the screw-based invariants.

B. Inter-sensor Agreement

To evaluate the effect of the sensor placement, speed and motion-type, we propose the correlation coefficients $R_{\bar{\omega}_1}$ and $R_{\bar{v}_1}$ for $\bar{\omega}_1$ and $\bar{v}_1$. These correlation coefficients for our dataset is succinctly summarised in Fig 9. Generally, a correlation coefficient of 0.8 or higher shows good temporal agreement between the compared signals.

For the basic motions, $R_{\bar{\omega}_1}$ shows very good agreement even at different speeds. However, the effect of motion speed on $R_{\bar{v}_1}$ shows random patterns. For complex motions, both $R_{\bar{\omega}_1}$ and $R_{\bar{v}_1}$ shows random effects. This means that during complex movements, it is very challenging to ensure high-reliability of the screw-based invariants. It might not be a limitation of the screw-based invariants themselves. Importantly, recent studies have shown that the dynamic accuracy of the off-the-shelf IMUs does depend on the motion-type [8]. This is why for complex motions, $R_{\bar{\omega}_1}$ for R-S1, R-S3 and R-S4 shows low correlation (see the beige coloured plot in Fig 9).

C. Measure of Reliability

Generally, it is very challenging to analyse the consistency or reliability of kinematic variables which are simultaneously extracted from different devices [18]. In such situations, simple summary statistics are an ineffective measure of kinematic reliability [18]. Therefore, we use the coefficient of multiple correlations (CMC) proposed by Ferrari et al. [18]. Here, the CMC measures the level of agreement or dispersion between the kinematic variables. For a waveform Y_{gpf} with G

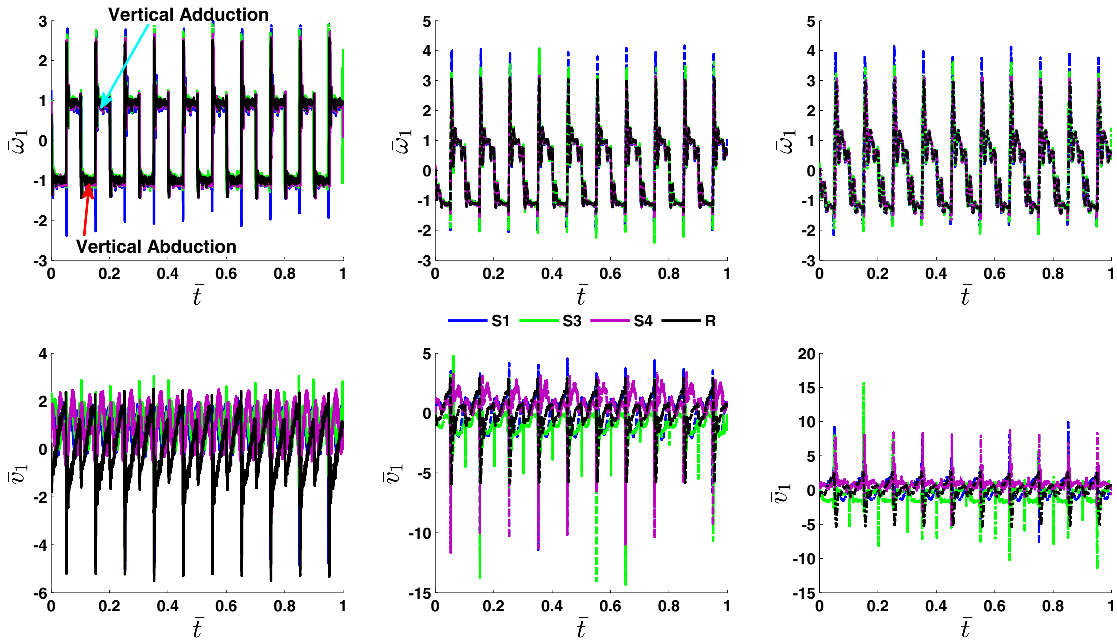

Figure 6: Plot shows the screw-based invariants extracted for the vertical abduction-adduction task. The various columns represent the slow (solid), medium (dashed) and fast (dash-dotted) for ten repetitions.

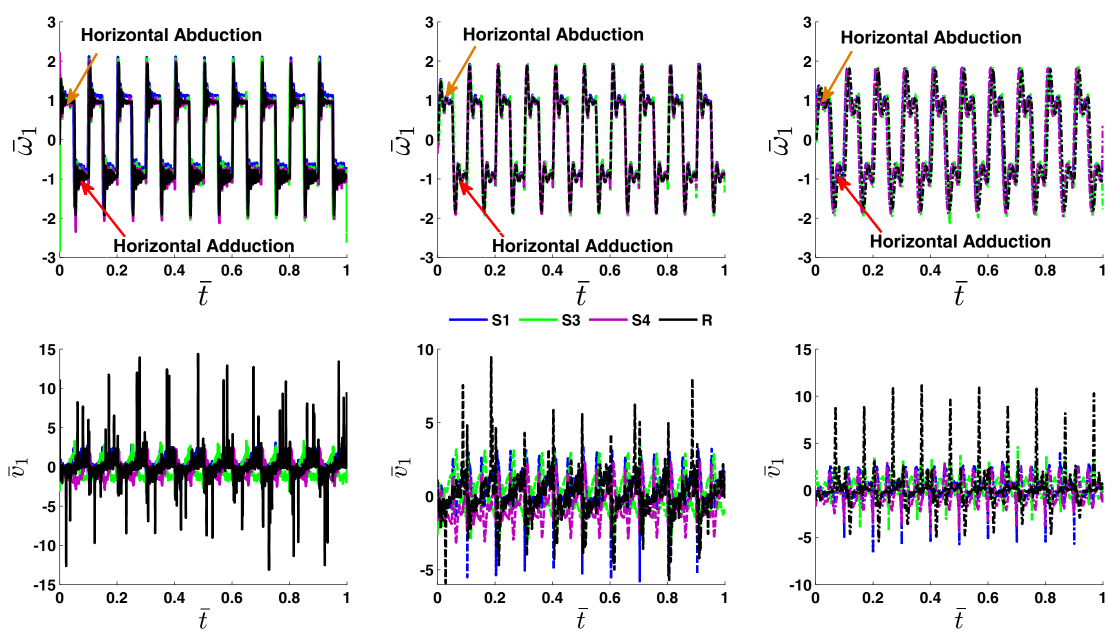

Figure 7: The plot shows the screw-based invariants extracted for the horizontal abduction-adduction task. The various columns represent the slow (solid), medium (dashed) and fast (dash-dotted) for ten repetitions.

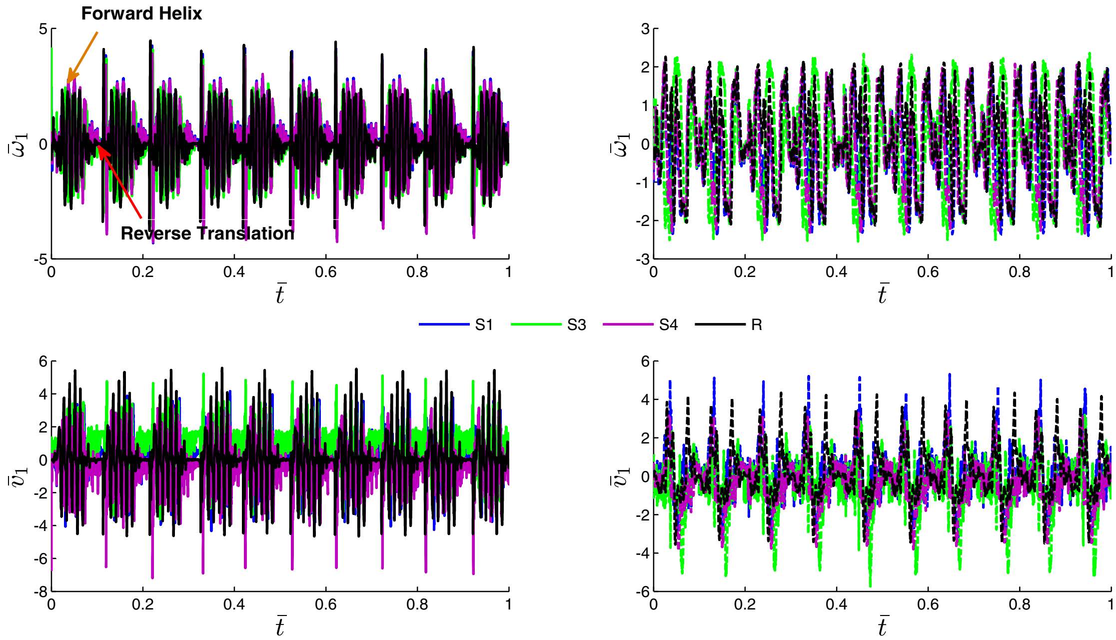

Figure 8: The plot shows the screw-based invariants extracted for the two advanced motions: helical trajectory (solid) and lemniscate trajectory (dashed) for ten repetitions.

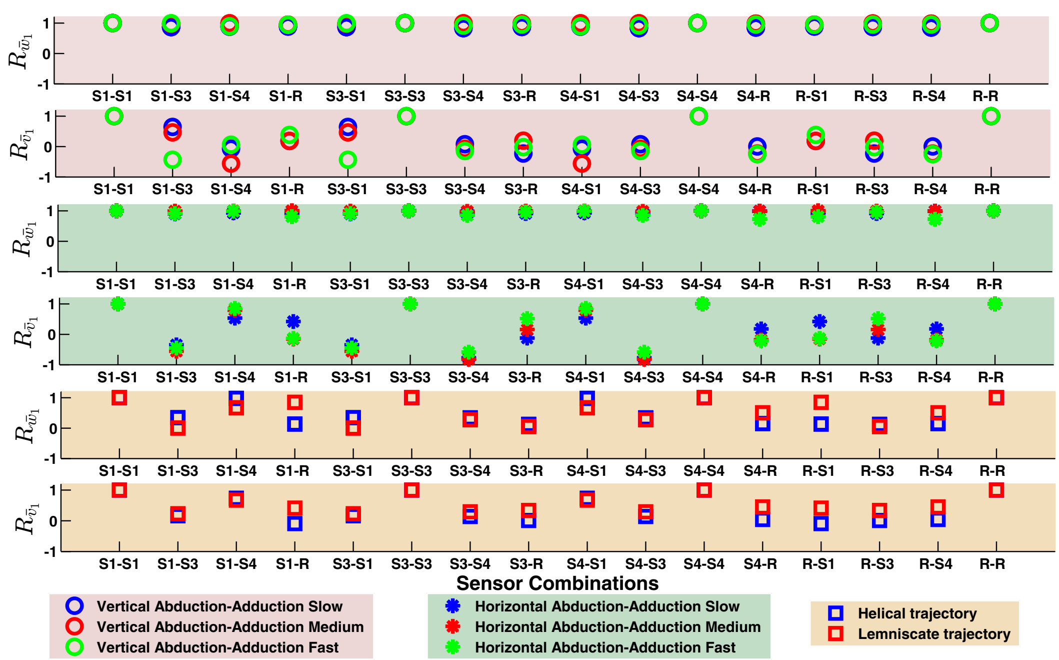

Figure 9: The plot presents the inter-sensor agreement between various IMU sensors (S1, S3, S4) and the robot (R) as the ground-truth. Here, $R_{\bar{\omega}_1}$ and $R_{\bar{v}_1}$ are the temporal correlation coefficients for the geometric invariants $\bar{\omega}_1$ and $\bar{v}_1$.

Table I: CMC values computed for different motion types and speeds.

Type	Speed	CMC $\bar{\omega}_1$	CMC $\bar{v}_1$
Vertical Abduction-Adduction	Slow	0.9296	0.1863i
	Medium	0.9876	0.3079i
	Fast	0.9695	0.3311i
Horizontal Abduction-Adduction	Slow	0.9566	0.2511i
	Medium	0.9933	0.3874i
	Fast	0.9347	0.0393i
Helical trajectory	—-	0.5795	0.3438
Lemniscate trajectory	—-	0.6063	0.6077

repetitions each consisting of F_g frames and P devices,

$$CMC = \sqrt{1 - \frac{\sum_{g=1}^{G}[\sum_{p=1}^{P}\sum_{f=1}^{F_g}(Y_{gpf} - \bar{Y}_{gf})^2]/GF_g(P-1)}{\sum_{g=1}^{G}[\sum_{p=1}^{P}\sum_{f=1}^{F_g}(Y_{gpf} - \bar{Y}_g)^2]/G(PF_g - 1)}}. \tag{9}$$

Here, $\bar{Y}_{gf}$ is the mean waveform in the cycle across the P devices and $\bar{Y}_g$ is the grand mean [18], where F_g changes with each G-th cycle. In general, a CMC value of the range of $0.85 - 0.94$ is considered to be very good and that of $0.95 - 1$ to be excellent. When the dispersion level among the waveforms is high, the CMC value becomes zero or a complex quantity [8], [18].

The computed CMC values for our dataset is summarised in Tab I. For basic motions, it is clear that the CMC for the invariant $\bar{\omega}_1$ shows very good to excellent reliability. Contrastingly, CMC values for $\bar{v}_1$ are highly unreliable which is very evident from the Fig 6 and Fig 7. For complex motions, the computed CMCs shows only a moderate reliability.

VII. Conclusions and Future Work

To conclude, through a series of experiments we have shown that the normalised screw-based invariant $\bar{\omega}_1$ can reliably segment the motion reversals of a rigid-IMU cluster. This is clear from the plots of $\bar{\omega}_1$ in Fig 6, Fig 7 and the computed CMC values for $\bar{\omega}_1$ for basic motions in Tab I. Moreover, we have shown that the reliability of $\bar{\omega}_1$ is unaffected by sensor placement or motion speed. However, the motion-type does affect the reliability of the geometric invariant $\bar{\omega}_1$. Note that the reliability of the geometric invariant $\bar{v}_1$ needs to be improved further. Therefore, in the near future, we aim to improve the velocity estimation from the raw accelerometer signals. In conclusion, we have shown that the screw-based invariants can reliably segment the motion reversals of a rigid-IMU cluster.

Acknowledgement

Silvia Cruciani is supported by the Swedish Foundation for Strategic Research project FACT

References

[1] D. Novak and R. Riener, "A survey of sensor fusion methods in wearable robotics." *Rob. Auton. Syst.*, vol. 73, pp. 155–170, 2015.

[2] D. Kulic, G. Venture, K. Yamane, E. Demircan, I. Mizuuchi, and K. Mombaur, "Anthropomorphic Movement Analysis and Synthesis: A Survey of Methods and Applications." *IEEE Trans. Robot.*, vol. 32, no. 4, pp. 776–795, aug 2016.

[3] S. O. H. Madgwick, A. J. L. Harrison, and R. Vaidyanathan, "Estimation of IMU and MARG orientation using a gradient descent algorithm," in *2011 IEEE Int. Conf. Rehabil. Robot.* IEEE, jun 2011, pp. 1–7.

[4] O. Lambercy, S. Maggioni, L. Lünenburger, R. Gassert, and M. Bolliger, "Robotic and Wearable Sensor Technologies for Measurements/Clinical Assessments," in *Neurorehabilitation Technol.* Cham: Springer International Publishing, 2016, no. 1, pp. 183–207.

[5] P. Picerno, "25 years of lower limb joint kinematics by using inertial and magnetic sensors: A review of methodological approaches," *Gait Posture*, vol. 51, pp. 239–246, 2017.

[6] M. Iosa, P. Picerno, S. Paolucci, and G. Morone, "Wearable inertial sensors for human movement analysis," *Expert Rev. Med. Devices*, vol. 13, no. 7, pp. 641–659, 2016.

[7] A. Filippeschi, N. Schmitz, M. Miezal, G. Bleser, E. Ruffaldi, and D. Stricker, "Survey of Motion Tracking Methods Based on Inertial Sensors: A Focus on Upper Limb Human Motion." *Sensors*, vol. 17, no. 6, p. 1257, 2017.

[8] K. Lebel, P. Boissy, H. Nguyen, and C. Duval, "Inertial measurement systems for segments and joints kinematics assessment: towards an understading of the variations in sensors accuracy." *Biomed. Eng. Online*, vol. 16, no. 1, p. 56, dec 2017.

[9] J. De Schutter, "Invariant Description of Rigid Body Motion Trajectories." *J. Mech. Robot.*, vol. 2, no. 1, p. 011004, 2010.

[10] R. Krishnan, N. Björsell, and C. Smith, "Segmenting Humeral Submovements using Invariant Geometric Signatures," in *2017 IEEE/RSJ Int. Conf. Intell. Robot. Syst.*, 2017.

[11] J. F. S. Lin and D. Kulic, "Online segmentation of human motion for automated rehabilitation exercise analysis." *IEEE Trans. Neural Syst. Rehabil. Eng.*, vol. 22, no. 1, pp. 168–180, 2014.

[12] A. Fod, M. J. Mataric, and O. C. Jenkins, "Automated derivation of primitives for movement classification." *Auton. Robots*, vol. 12, no. 1, pp. 39–54, 2002.

[13] T. Aoki, J. F.-S. Lin, D. Kulic, and G. Venture, "Segmentation of human upper body movement using multiple IMU sensors," in *2016 38th Annu. Int. Conf. IEEE Eng. Med. Biol. Soc.*, no. 2. IEEE, aug 2016, pp. 3163–3166.

[14] R. Soloperto, M. Saveriano, and D. Lee, "A bidirectional invariant representation of motion for gesture recognition and reproduction," *Proc. - IEEE Int. Conf. Robot. Autom.*, vol. 2015-June, no. June, pp. 6146–6152, 2015.

[15] V. Bonnet, C. Mazza, P. Fraisse, and A. Cappozzo, "Real-time estimate of body kinematics during a planar squat task using a single inertial measurement unit," *IEEE Trans. Biomed. Eng.*, vol. 60, no. 7, pp. 1920–1926, 2013.

[16] K. Tong and M. H. Granat, "A practical gait analysis system using gyroscopes," *Med. Eng. Phys.*, vol. 21, no. 2, pp. 87–94, 1999.

[17] U. X. Tan, K. C. Veluvolu, W. T. Latt, C. Y. Shee, C. N. Riviere *et al.*, "Estimating displacement of periodic motion with inertial sensors," *IEEE Sens. J.*, vol. 8, no. 8, pp. 1385–1388, 2008.

[18] A. Ferrari, A. G. Cutti, and A. Cappello, "A new formulation of the coefficient of multiple correlation to assess the similarity of waveforms measured synchronously by different motion analysis protocols." *Gait Posture*, vol. 31, no. 4, pp. 540–542, 2010.